

Bifurcation structure and chaos in nanomagnet coupled to Josephson junction

M. Nashaat^{1,2}, M. Sameh¹, A. E. Botha³, K. V. Kulikov^{2,4}, and Yu. M. Shukrinov^{2,4,5}

¹ *Department of Physics, Faculty of Science, Cairo University, 12613, Giza, Egypt*

² *BLTP, JINR, Dubna, Moscow Region, 141980, Russia*

³ *Department of Physics, University of South Africa, Johannesburg 1710, South Africa*

⁴ *Dubna State University, Dubna, Moscow Region, Russia*

⁵ *Moscow Institute of Physics and Technology, Dolgoprudny, 141700, Russia*

(Dated: November 25, 2021)

Recently an irregular easy axis reorientation demonstrating the Kapitza pendulum features were observed in numerical simulations of nanomagnet coupled to the Josephson junction. To explain its origin we study the magnetization bifurcations and chaos which appear in this system due to interplay of superconductivity and magnetism. The bifurcation structure of the magnetization under the variation of Josephson to magnetic energy ratio as a control parameter demonstrates several precessional motions. They are related to chaotic behavior, bistability, and multiperiodic orbits in the ferromagnetic resonance region. Effect of external periodic drive on the bifurcation structure is investigated. The results demonstrate high-frequency modes of periodic motion and chaotic response near resonance. Far from the ferromagnetic resonance we observe a quasiperiodic behavior.

I. INTRODUCTION

Spintronics is currently the main contender for next-generation nanoscale devices, aiming for faster processing speeds and lower power consumption [1]. On the other hand, superconductors stand out as ultra-low energy dissipation systems. Superconductivity thus has the potential to reduce inherent heating effects in spintronic devices. As such, many different approaches have been developed to enhance spintronic effects through the incorporation of superconductivity, and to understand the interactions that arise due to the coexistence of superconducting and magnetic states. Such efforts have spawned the relatively new field of superconductor spintronics [2, 3].

Molecular nanomagnets [4–6] are good candidates for qubit realization, due to their long magnetization relaxation time [7–10]. Hybrid structures, such as the nanomagnet coupled to Josephson junction (NM-JJ), are also important contenders for the development of spintronic devices [11, 12]. The dynamics of magnetic nanoparticles and that of the JJ are separately governed by nonlinear differential equations. The magnetic nanoparticle can be described by the Landau–Lifshitz–Gilbert equation [13], while, the Josephson junction, can be described by the resistively and capacitively shunted Josephson junction (RCSJ) model [14].

The coupling in JJ-NM system may be established in different ways, particularly, through the spin orbit coupling in φ_0 -junction [15]. Another type of coupling is realized in NM-JJ, where the electromagnetic coupling between spin-wave and Josephson phase takes place [17–24].

The nonlinear dynamics of the JJ is sensitive to the orientation of the magnetization [16, 25–31], and a rich physics has been predicted due to this type of coupling between the Josephson and magnetic subsystems: for example, supercurrent-induced magnetization dynamics

[25, 32, 33]. In the NM-JJ system, the reversal of the magnetic moment by the supercurrent pulse [30], the appearance of Devil’s staircase [24] and Kapitza pendulum effects [11, 34, 35], have been investigated.

In Ref. [11, 35], the authors introduced the Kapitza pendulum as a mechanical analog to the NM-JJ system and demonstrated the reorientation of the easy axis of the magnetic moment of the nanomagnet. In this case, the Josephson to magnetic energy ratio G plays the role of the drive amplitude of the variable force and Josephson frequency Ω_J plays the role of the drive frequency in the Kapitza problem. The average magnetization component m_z characterizes the changes of the stability position. However, at present, to the best of our knowledge, there is no systematic study of the nonlinear dynamic features in the NM-JJ systems. Therefore, in this article, the dynamical equations which describe the coupling in this system in the framework of the voltage biased Josephson junction is studied. We investigate the magnetization bifurcations and chaos which appear in this system due to interplay of superconductivity and magnetism, and calculate the bifurcation diagrams, Lyapunov exponents and Poincaré sections. The several precessional motions related to chaotic behavior, bistability, and multiperiodic orbits in the ferromagnetic resonance region (FMR) are demonstrated. Chaos driven by the external periodic drive is also investigated. An estimation of the model parameters shows that there is a possibility for the experimental observation of the predicted phenomenon.

The plan of the rest of the paper is as follows. In Sec.II, we describe the model and present an estimation of the model parameters. The dynamics and reorientation features of the nanomagnet coupled to Josephson junction is demonstrated in Sec.III. This is followed by a discussion of the bifurcation diagrams and Poincaré sections. In Sec.IV we discuss the chaos driven by an external periodic drive. Here, the appearance of the quasiperiodic motion is presented also. Finally, we conclude in Sec.V.

II. MODEL

We consider short Josephson junction (JJ) with length l coupled to a single-domain nanomagnet with magnetization \mathbf{M} and easy axes in y -direction. The nanomagnet is located at distance $r_M = a\hat{e}_x$ from the center of the junction as shown in Fig.1. The magnetic field of the nanomagnet alters the Josephson current, while the magnetic field generated by the Josephson junction acts on the magnetization of the nanomagnet. Thus, an electromagnetic interaction between the JJ and nanomagnet is occurred.

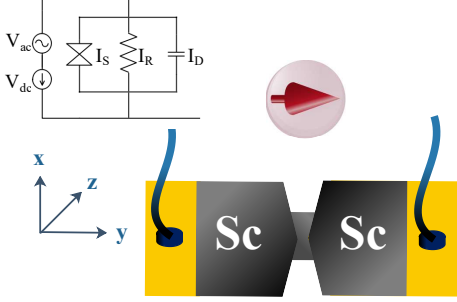


Figure 1. Schematic diagram of the system of JJ-NM with the system geometry. In the equivalent circuit, V_{dc} is the bias voltage, V_{ac} is the ac external drive, I_s is the superconducting current, I_R is the resistive current, and I_D is the displacement current.

The magnetization dynamics in such system can be described by the Landau-Lifshitz-Gilbert (LLG) equation [36, 37]:

$$\frac{d\mathbf{M}}{dt} = -\gamma \mathbf{H}_{eff} \times \mathbf{M} + \frac{\alpha}{M_0} \left(\mathbf{M} \times \frac{d\mathbf{M}}{dt} \right), \quad (1)$$

where α is the Gilbert damping parameter, which is a property of the material and lies between 0.0001 and 0.1 for most ferromagnetic materials [38, 39], and γ is the gyromagnetic factor. The effective field in LLG equation is given by [15]:

$$\mathbf{H}_{eff} = -\frac{1}{V_F} \frac{\partial E}{\partial \mathbf{M}}, \quad (2)$$

where V_F is the volume of the nanomagnet, and the total energy (E) of the system is the sum of magnetic anisotropy energy (E_M), Josephson energy (E_J), and Zeeman energy (E_Z). The first two terms are given by

$$E_M = -\frac{K_{an} V_F}{2} \left(\frac{M_y}{M_0} \right)^2, \quad (3)$$

$$E_J = \epsilon_J \left[1 - \cos \left(\frac{2\pi}{\Phi_0} vt + \varphi_m \right) \right]. \quad (4)$$

Here K_{an} is the magnetic anisotropy constant, $M_0 = |\mathbf{M}|$ is the saturation magnetization, $\epsilon_J =$

$\Phi_0 I_c / 2\pi$, I_c is critical current of the JJ, Φ_0 is the flux quantum, and v is the bias voltage for JJ. The phase shift φ_m is induced due to mutual interaction of the nanomagnet and JJ. This shift can be calculated from the vector potential $\mathbf{A}_m(\mathbf{r}, t)$ which takes into account the magnetic field of the nanomagnet created at point \mathbf{r} and external magnetic fields if considered (see refs. [12, 35] for detail). According to this, the shift is given by [12]:

$$\begin{aligned} \varphi_m &= -\frac{2\pi}{\Phi_0} \int d\mathbf{l} \cdot \mathbf{A}_m(\mathbf{r}, t) = -km_z, \\ \mathbf{A}_m(\mathbf{r}, t) &= \frac{\mu_0}{4\pi} \frac{\mathbf{M} \times \mathbf{r}}{r^3}, \\ k &= \frac{2\pi}{\Phi_0} \frac{\mu_0 M_0 l}{a\sqrt{a^2 + l^2}}, \end{aligned} \quad (5)$$

where the integration goes from one side of the junction to the other side, μ_0 is the permeability of free space and k play the role of the coupling in the proposed system. The last term which contributes to the total energy is generated by the normal current and is given by [12, 35]:

$$E_z = -I_N \int d\mathbf{l} \cdot \mathbf{A}_m(\mathbf{r}, t). \quad (6)$$

where in the dimensionless form $I_N = [V - kn\dot{z}]$, and $V = v/I_c R$ is the normalized voltage. In our normalization $V = \Omega_J$, $\Omega_J = \omega_J/\omega_c$, ω_J is the Josephson frequency $\omega_J = 2\pi v/\Phi_0$, $\mathbf{m} = \mathbf{M}/M_0$, t is normalized to ω_c^{-1} , $\omega_c = 2\pi I_c R/\Phi_0$ is the Josephson characteristic frequency, R is the junction resistance, ω_F is the ferromagnetic resonance frequency, $\Omega_F = \omega_F/\omega_c$, and the effective field \mathbf{h}_{eff} is normalized to magnetic anisotropy field. According to this, the LLG reads as

$$\frac{d\mathbf{m}}{dt} = -\frac{\Omega_F}{(1 + \alpha^2)} \left(\mathbf{m} \times \mathbf{h}_{eff} + \alpha [\mathbf{m} \times (\mathbf{m} \times \mathbf{h}_{eff})] \right), \quad (7)$$

with,

$$\begin{aligned} h_y &= m_y, \quad h_z = \tilde{h}_z - \epsilon k m_z \\ \text{and} \quad \tilde{h}_z &= \epsilon [\sin(\Omega_J t - km_z) + \Omega_J]. \end{aligned} \quad (8)$$

where h_y , h_z are the components of the effective field in the y - and z -direction respectively, $\epsilon = Gk$, $G = \epsilon_J/K_{an}V_F$ is the Josephson to magnetic energy ratio.

For experimental realization of such a system, we introduce approximate estimations for the model parameters based on Refs.[40–43]. We present in Table.I estimations for typical Josephson junctions, in Table.II for typical nanomagnet parameters, and in Table.III for model parameters. The value of k depends on the distance of the nanomagnet from the JJ and the length of the junction (here, for estimation we consider $a = 250\mu m$). Experimental results give the estimation for the ferromagnetic resonance frequency of nanomagnets within the range of $\sim 5 - 10GHz$ [44, 45]. In the voltage-biased Josephson junction, one can tune the Josephson frequency in a wide region around the FMR.

Table I. Typical Josephson junctions parameters

Parameter	$Al/Al_2O_3/Al$	$Nb/Al_2O_3/Nb$
l	141 nm	20 nm
I_c	20 nA	6 mA
ϵ_J	6.58×10^{-24} J	2.19×10^{-18} J
R	10 k Ω	0.003 Ω
ω_c	~ 600 GHz	~ 50 GHz

Table II. Parameters

Parameter	Material
M_0	907 kA/m ($SmCo_5$),
	1950 kA/m ($Fe_{65}Co_{35}$)
K_{an}	17000 kJ/m ³ ($SmCo_5$),
	20 kJ/m ³ ($Fe_{65}Co_{35}$)
v	~ 1.979 m ³ $\times 10^{-23}$

Table III. Model parameters

Parameter	$Al/Al_2O_3/Al$	$Nb/Al_2O_3/Nb$
k	0.01	0.01
G	0.0001	5.5,
		10π ($v \sim 120$ nm ³) and $k_{an} = 10$ kJ/m ³

The results presented in the paper have been obtained using different numerical methods. In particular, we solve Eq.(1) numerically using implicit Gauss-Legendre method [46] to calculate the dynamics of the system. To characterize different kind of motions the bifurcation diagram, the Poincaré sections and the largest Lyapunov exponent (LLE) have been calculated. In this case, we solve the system of equations (1) in the fixed time interval which is multiplied to the drive period ($2\pi/\Omega_J$) with the time step equals to $\sim 10^{-4}$. The number of time steps in our time domain is equal 10^8 . Then, we save the values of the components m_x , m_y , and m_z at the end of the time interval, those points also create the Poincaré section for trajectories in phase space. To find the LLE as a function of G , we calculate the magnetic moment dynamics with the initial conditions $m = (0, 1, 0)$, then randomly shift them ($\delta \approx 10^{-5}$) from the reference one. Then, we calculate the LLE from m_x, m_y, m_z and $m_x + \delta, m_y + \delta, m_z + \delta$ and average it over time. Of course, different initial conditions can lead to slightly different pictures, but the qualitative picture remains the same. The LLE is used to determine the sensitivity of the system to the initial conditions. The positive LLE is one of the signs of chaos in the system, this means that two phase space trajectories with a small difference in initial conditions will rapidly diverge, and then have totally different futures. The negative value of LLE indicates that the system approaches a fixed point (here the fixed point is $(0, 0, 1)$ for which $\langle m_z(t) \rangle = 1$). The zero value of LLE shows that the system is periodic or quasiperiodic.

We consider the ferromagnetic resonance frequency $\Omega_F = 1$, the coupling constant between the JJ and the nanomagnet $k = 0.05$, and the Gilbert damping parameter $\alpha = 0.1$. We have chosen the Josephson to magnetic energy ratio G and the Josephson frequency Ω_J as control parameters, which represents an experimentally reasonable choice. All our calculations start with minimum value of $G = 0.01\pi$.

III. IRREGULAR REORIENTATION BEHAVIOR, BIFURCATIONS AND CHAOS

In the proposed model, the magnetic field of the total tunneling current (both the superconducting and quasiparticle) have been taken into account. This leads to the two different reorientation mechanisms of the nanomagnet easy axis. One mechanism is related to the magnetic field, created by the quasiparticle current flowing through the JJ. The other one is related to the oscillating magnetic field generated by the superconducting current. The second one is a manifestation of Kapitza pendulum-like feature which was observed in the magnetization dynamics of the nanomagnet [11, 35] and φ_0 -junction [34].

Figure 2 shows the average magnetic moment component m_z as a function of the Josephson to magnetic energy ratio G . One can see the smooth change of $\langle m_z(t) \rangle$ from zero to one as a function of G at $\Omega_J = 5$. The stabilization of the magnetic moment components dynamics occurs at $M = (0, 0, 1)$, when G exceeds a certain reorientation value, which indicates a complete reorientation of the magnetic moment. Notice that for $\Omega_J \simeq \Omega_F$ the fluctuations of $\langle m_z(t) \rangle$ appear before the complete reorientation. To understand the origin of the fluctuations at the FMR, we investigate the dynamics of the effective field and the transformations of the magnetic moment dynamics for two cases, one at the FMR, the other far away.

The dynamics of the effective field components $h_y(t)$ and $h_z(t)$ as functions of G at $\Omega_J = 1$ and $\Omega_J = 5$ are demonstrated in Fig. 3. As we see, there is no temporal dependence of $h_y(t)$ and $h_z(t)$ at a small $G \ll 1$ (the curve with $G = 0.01\pi$) since the Josephson energy is too small in compare to anisotropy energy and its magnetic field does not affect the nanomagnet. The temporal dependence of $h_y(t)$ at $G > 1$ demonstrates irregular oscillations with different amplitudes at $\Omega_J \simeq \Omega_F$ (see Fig.3(a-i)) and regular oscillations at $\Omega_J > \Omega_F$ (see Fig.3(b-i)). On the other hand, the temporal dependence of $h_z(t)$ shows a periodic structure (see Fig.3(a-ii) and Fig.3(b-ii)) with amplitude which increases with the increasing in G at fixed Ω_J . The stabilization of the magnetic moment dynamics occurs at $M = (0, 0, 1)$, when G exceeds a certain reorientation value, which indicates a complete reorientation of the magnetic moment. The value of G at which the complete reorientation occurs decreases with increasing Ω_J .

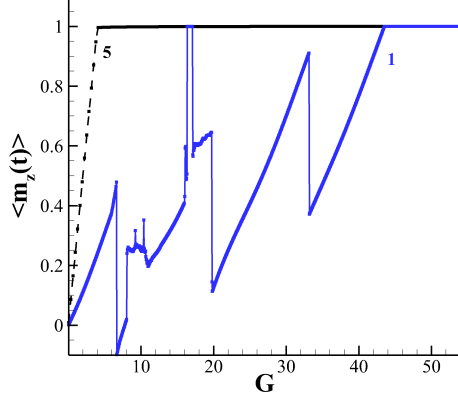


Figure 2. The average magnetization component $\langle m_z(t) \rangle$ as a function of G , demonstrating the Kapitza pendulum-like features in NM-JJ system [11, 35]. The blue solid line indicate the results calculated at $\Omega_J = 1$. The black dashed line at $\Omega_J = 5$.

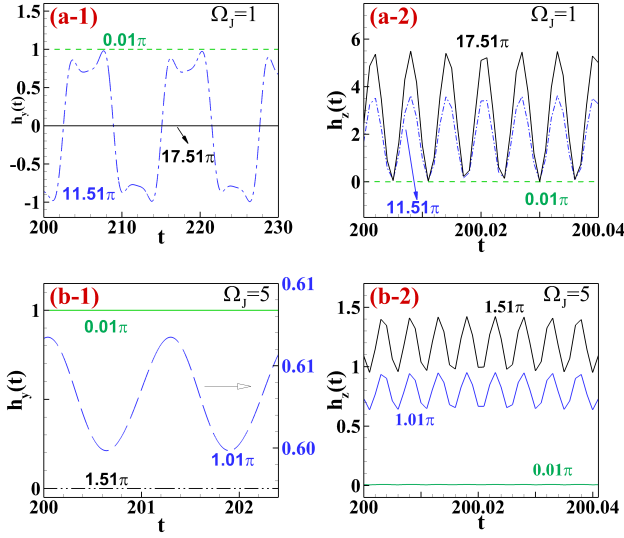


Figure 3. The temporal dependence of effective field components as a function of G : (a-1) $h_y(t)$ and (a-2) $h_z(t)$ at $\Omega_J = 1$, (b-1) $h_y(t)$ and (b-2) $h_z(t)$ at $\Omega_J = 5$. The numbers indicate the value of G .

The dynamical behavior of $h_y(t)$ and $h_z(t)$ reflects on the average value of the effective field components. Therefore, we investigate h_{y-av} and h_{z-av} as functions of G and Ω_J and create 2-D maps, which are demonstrated in Fig. 4(a and b). Fig. 4(a) shows that the average of h_y has a non-zero values only at $G < 20\pi$ and around the FMR condition ($\Omega_J \simeq \Omega_F$), while the average of h_z smoothly increasing with the increasing in G and Ω_J (see Fig.4(b)). We note that the condition $h_{y-av} = 0$ indicates the complete reorientation of the magnetic moment, while the negative values of h_{y-av} indicates the re-

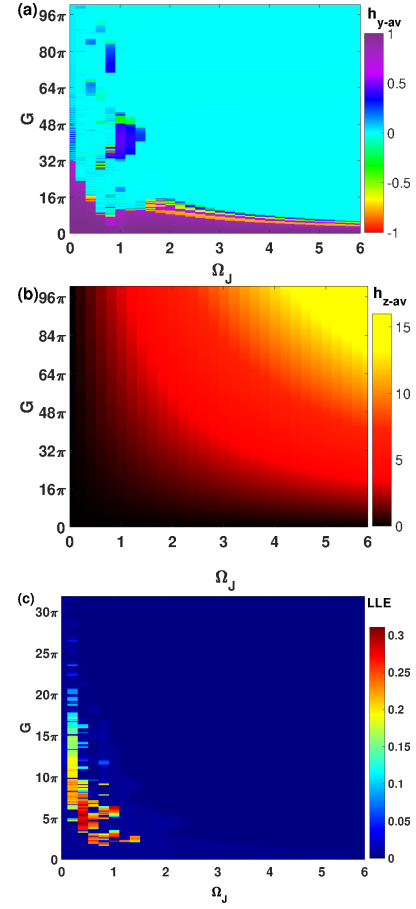


Figure 4. (a) The average value of h_{y-av} , (b) the average value of h_{z-av} and (c) the largest Lyapunov exponent as functions of G and Ω_J .

versal of the easy axis [11, 12]. The reorientation features at $\Omega_J \gg \Omega_F$ have been investigated in Refs. [11, 35]. Here, we investigate the regions of the non-zero values of h_{y-av} which appear at small Ω_J ($\Omega_J < 2$). The system in this region is influenced by the irregular oscillations of $h_y(t)$, which can be a cause of a chaotic dynamic of the nanomagnet. So, we calculated the LLE as functions of G and Ω_J . The results of our calculation is presented in Fig.4(c). The LLE shows a non zero value at $\Omega_J \simeq \Omega_F$. Therefore, the system may demonstrates a chaotic response in this interval of frequencies.

A. Dynamical effects at $\Omega_J = 1$

To confirm the chaotic nature of the magnetic moment dynamics we calculate the bifurcation diagrams. The bifurcation diagrams reveal structural changes of the motion in the parameter space [39].

Figs.5 (a-c) show the bifurcation trees of the magnetization as a functions of G (at the FMR $\Omega_J = \Omega_F$) before the complete reorientation of the easy axis. The bifurcation tree starts from the fixed point (FP) ($m_y = 1$) and

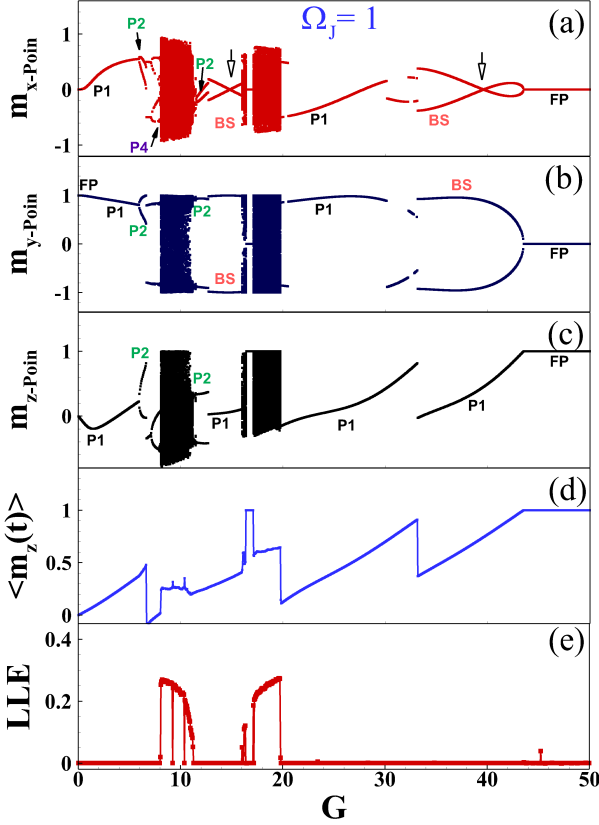


Figure 5. Bifurcation diagram of the magnetization components (a) m_x , (b) m_y , (c) m_z , (d) the average value of m_z -component and (e) the largest Lyapunov exponent as a function of G at $\Omega_J = 1$.

demonstrates a period-1 (P1) motion (0-branch on the bifurcation tree) at $G < 6$. The first period doubling (or the 1st branch) occurs at $G = 6$ and the system starts to perform period-2 (P2) motion up to $G < 7.9$. Second period doubling is observed at $G = 7.9$ (period-4 (P4) motion). Then, chaotic bands can be observed at the intervals $[8, 11.5]$ and $[16, 20]$, with the periodic motion in between. The system demonstrates a bistable state (BS), two points with the same value, but different signs, for m_x and m_y within the intervals $[12.7, 16]$ and $[30, 43.5]$, while m_z shows the regular P1 motion. In addition to this, two folding bifurcation are revealed (indicated by the hollow arrows in Fig5(a)). Finally, the system approaches the stable FP at $G \geq 43.5$, corresponding to the complete reorientation of the easy axis $m_z = 1$.

The system transition from one kind of motion to another is accompanied by abrupt changes in the average magnetization components. We demonstrate such changes in Fig.5(d), where the irregular reorientation behavior of $\langle m_z(t) \rangle$ appears before the complete reorientation. The LLE calculation confirms the chaotic behavior of the magnetization (see Fig.5(e)). The positive values intervals of LLE coincide with the chaotic bands

observed in the bifurcation diagrams.

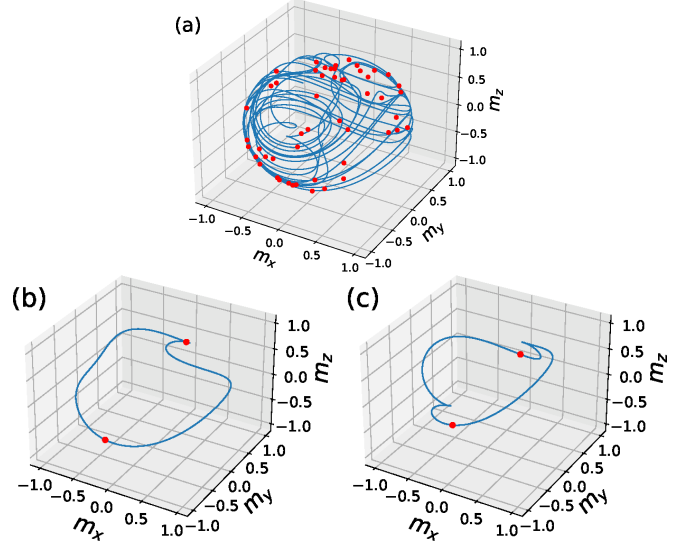


Figure 6. Orbits of motion (blue curve) of the system and corresponding Poincaré section (red dots). (a) at $G = 9$ with chaos, (b) at $G = 12$ with P2 motion, (c) at $G = 14$ with bistable states in m_x and m_y , and P1 motion in m_z . All panels are done at $\Omega_J = 1$.

To support our conclusions, concerning the chaotic behavior, we also calculate the Poincaré sections along with the orbits of motion at specific values of G and results presented in Fig. 6. The Poincaré sections with one point only indicates that the magnetization exhibits P1 motion, two points – P2 motion, and so on. The magnetization dynamics shows the dense and random distribution of the trajectories and the Poincaré section points at $G = 9$ (see Fig. 6(a)). This along with the positive LLE and dense distribution of points on the bifurcation diagram confirm the chaotic nature of those states. Fig. 6(b) demonstrates the trajectories and the Poincaré section points of the P2 motion at $[11.5, 12.7]$. However, two points in the Poincaré section can also indicate BS, as it is presented in Fig. 6(c), where m_x and m_y show BS and P1 motion in m_z at $[12.7, 16]$ in the bifurcation diagram. In BS the trajectory reaches a limit cycle near the $\pm y(x)$ -axis depending on the initial condition.

B. Dynamical effects at $\Omega_J = 1.5$

Next, we investigate the transformation of the magnetic moment dynamics from the case $\Omega_J = \Omega_F = 1$ to $\Omega_J \simeq \Omega_F$. Figs.7 (a-c) show the bifurcation trees of the magnetization as a functions of G at $\Omega_J = 1.5$. In this case a simpler bifurcation structure is observed for precessional motion in compared to $\Omega_J = 1$. The bifurcation trees at $\Omega_J = 1.5$ demonstrate only the periodic motions of different order, BS and FP and the LLE equals zero within the whole calculation range. The average $\langle m_z(t) \rangle$ as a function of G presented in Fig.7(d)

reflects the transition of the system from one kind of motion to another one.

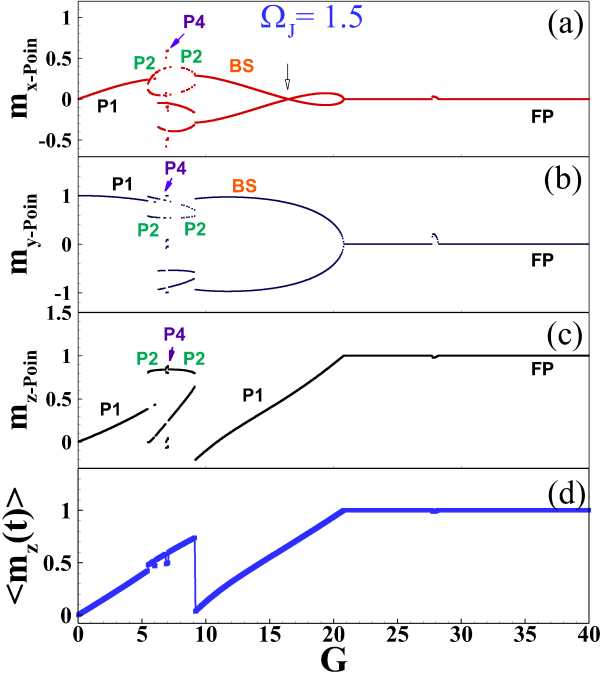


Figure 7. Bifurcation diagram of the magnetization components (a) m_x , (b) m_y , (c) m_z and (d) the average value of m_z -component as functions of G at $\Omega_J = 1.5$.

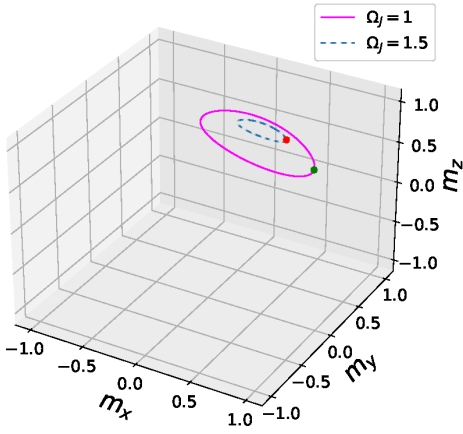


Figure 8. Orbits of the motion of the magnetization (dashed line for $\Omega_J = 1.5$, solid line for $\Omega_J = 1$) and corresponding Poincaré sections.

Figure 8 demonstrates a shrinking of orbits of motion under the increase of Ω_J . The increases of the driving frequency Ω_J reduces also the value of G at which the complete reorientation occurs (see dashed line in Fig. 2) [11, 35]. So, only the P1 motion before the stable FP can be observed at $\Omega_J = 5$.

In the considered system, the precession of the magnetization is driven by Josephson oscillations. So, the

increase in Ω_J forces the magnetization to follow the Josephson oscillations, and only the periodic motion can be observed. Therefore, it is the reason why we do not observe any chaotic behavior of the magnetization at $\Omega_J \geq 1.5$.

IV. CHAOS DRIVEN BY EXTERNAL PERIODIC DRIVE

In this section, we investigate the effect of the external periodic drive (PD) on the magnetization dynamics. In this case the total bias voltage for JJ consists of the dc and ac parts $V_{total} = V + A \cos(\Omega_r t)$, where A is the amplitude of the external radiation normalized to $\hbar\omega_c/2e$ and Ω_r is the frequency of the ac voltage normalized to ω_c . Therefore, the total tunneling current in the JJ is calculated in the framework of RCSJ-model:

$$I(t) = \sin\left(\Omega_J t - km_z + \frac{A}{\Omega_r} \sin(\Omega_r t)\right) + \Omega_J + A \cos(\Omega_r t) - k \frac{dm_z}{dt} - \beta_c A \Omega_r \sin(\Omega_r t). \quad (9)$$

The effective field components remain the same as in Eq.(8) except \tilde{h}_z which is given by:

$$\tilde{h}_z = \epsilon \left\{ \sin\left(\Omega_J t - km_z + \frac{A}{\Omega_r} \sin(\Omega_r t)\right) + \Omega_J + A \cos(\Omega_r t) - \beta_c A \Omega_r \sin(\Omega_r t) \right\}, \quad (10)$$

where β_c is the McCumber's parameter and the higher-order term ($-\beta_c k \ddot{m}_z$) is neglected. In this case, the nanomagnet effective field includes two oscillatory terms. One is the oscillating magnetic field, generated by the superconducting current, with the amplitude proportional to G and with the frequency of Josephson oscillations. The other one is the PD term. The main oscillatory mechanism is determined by the amplitudes of those terms.

A. Bifurcation structure as a function of G

First, we investigate the effect of G on the bifurcation structure under external PD. Figure 9 shows the bifurcation diagram of the magnetization dynamics and *LLE* at $\Omega_J = 1$, $\Omega_r = 0.8$ and $A = 1$. The bifurcation trees, in this case, starts from the P5 motion as a result of the influence of the external periodic drive (see Fig.9(a)). The magnetization dynamics undergoes the first period doubling at [2.4, 3.3] and after that the system returns back to P5 motion at [3.3, 3.8]. Then, the chaotic band can be observed at the interval [3.8, 16], where the *LLE* values at [3.9, 16] are on the order of 10^{-1} (see Fig.9(d)). Inside this chaotic band, there are very narrow windows of periodic motion at several values of G , where the P10 motion is observed. Those windows can be distinguished on the *LLE* as a corresponding dips near zero within [10, 15].

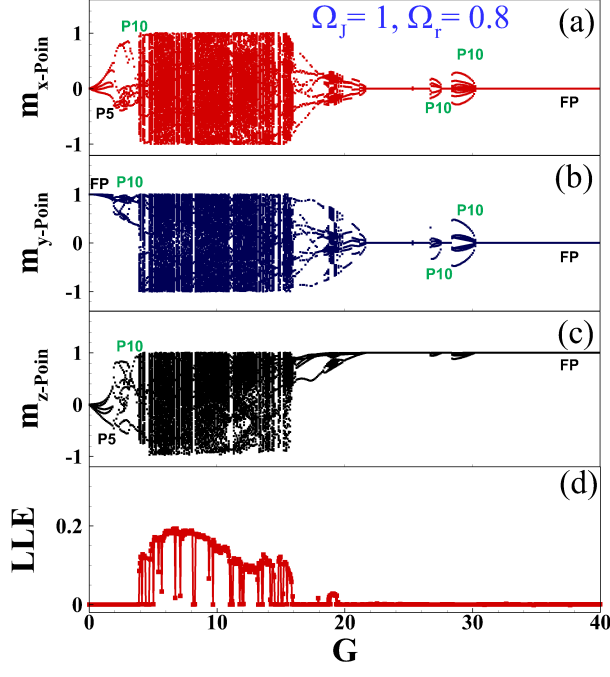


Figure 9. Bifurcation diagrams of the magnetization components (a) m_x , (b) m_y , (c) m_z and (d) the largest Lyapunov exponent as functions of G at $\Omega_J = 1$ under external periodic drive with $\Omega_r = 0.8$ and $A = 1$.

A small region of periodic motion with the high order modes is observed at $[18.4, 19.4]$. It is hard to recognize the oscillation modes in this crowded region due to the dense Poincaré section points within a small portion of the phase space. However, the LLE confirms the periodic nature of motion in this interval since the largest value is on the order of 10^{-2} (see Fig.9(d)), which is still small compared to the values of LLE where the chaotic behavior observed. The P5 motion appears at $G \geq 19.4$ and the magnetization dynamics approaches FP at $G \geq 21.7$ which is confirmed by the negative value of LLE in this region (see Fig.9(d)). However, the system does not settle and shows the P10 motion at the intervals $[25.3, 25.5]$, $[26.6, 27.6]$, and $[28.4, 30.5]$. After that the trajectory finds a stable FP corresponding to a complete reorientation of the magnetization direction ($\langle m_z(t) \rangle = 1$) at $G \geq 30.5$. So, the external periodic drive leads to a higher order periodic motion in the system. Notice also that in contrast to the case without external PD, the bifurcation diagrams do not show bistable states of the system throughout the whole range of G under investigation.

B. Bifurcation structure as a function of A

Significant changes in the bifurcation structure can be seen with increasing the amplitude A of external PD. So, we studied the effect of A as a control parameter on the

bifurcation diagram which is shown in Fig.10(a-c). The figure shows that starting from P1 motion at $A = 0, G = 5$ (see Fig. 5(a-c)), the system dynamics transforms into the higher order periodic motion at $0 < A \leq 0.2$. Then, several chaotic bands is observed in the intervals $[0.2, 7]$ and $[27, 29]$ with a small windows of higher order periodic motion in between.

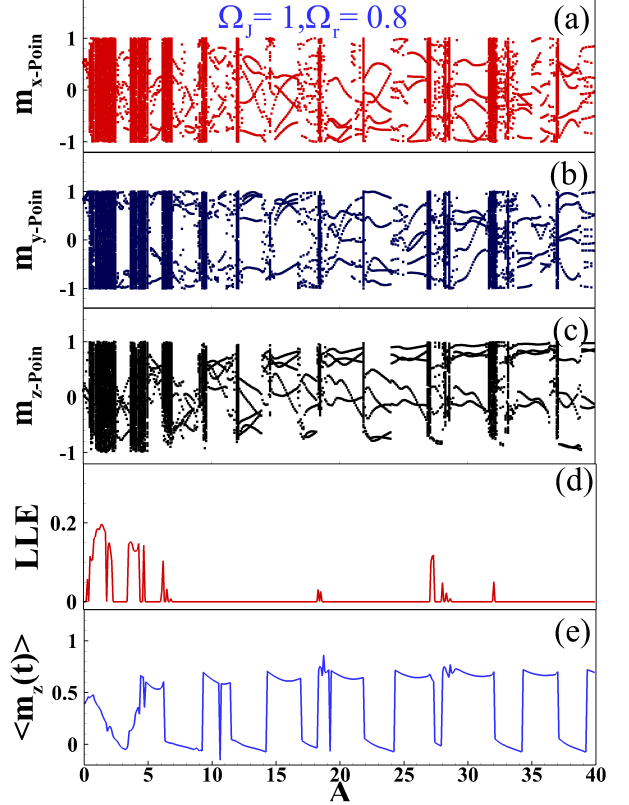


Figure 10. Bifurcation diagram of the magnetization components (a) m_x , (b) m_y , (c) m_z , (d) the largest Lyapunov exponent and (e) average value of m_z -component as functions of A at $\Omega_r = 0.8$, $\Omega_J = 1$ and $G = 5$.

The transitions between those states manifested in the LLE (see Fig. 10(d)) where the positive values indicate a strong chaotic response. We note also that the increase in the amplitude A changes the reorientation value (see Fig. 10(e)) as it have been discussed in Ref.[35], but at the given simulation parameters a complete reorientation of the easy-axis does not occur. By changing the amplitude of the external PD, one can transform the dynamics from chaotic region to higher order periodic one. Therefore, in NM-JJ system one can control the chaotic behaviour in the magnetization dynamics and reorientation process of the easy-axis.

The NM-JJ system under the external PD reveals another interesting long-term behavior far from the FMR region. Namely, the quasiperiodicity is mostly appears in the weak coupling regime (at a small G). In this case,

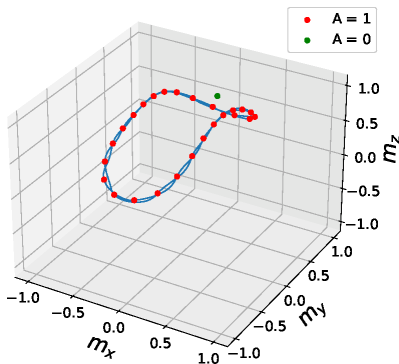


Figure 11. The Poincaré section (green dot) with P1 motion at $A = 0$ together with the quasiperiodic orbit (blue curve) and corresponding Poincaré section (red dots) at $\Omega_r = 0.8$, $A = 1$. Both panels are calculated at $\Omega_J = 5$ and $G = 3$.

the trajectories will never close into themselves. Fig. 11 demonstrates the transformation of the trajectory from the P1 motion (green dot) to the quasiperiodic one (blue curve with red dots) under the influence of PD at $G = 3$ and $\Omega_J = 5$.

V. CONCLUSIONS

We have provided a detail map of various types of motions in magnetization dynamics of the nanomagnet coupled to Josephson junction. The fluctuations in the reorientation process of the easy-axis caused by the transformations between the different types of motions of the system were demonstrated. The analysis of the bifurcation diagrams revealed the exact regions where the magnetization exhibits such motions. The chaotic states, bistability, and multiperiodic orbits have been demonstrated in the resonance region. When the Josephson frequency is larger than the resonance frequency, then the bistable states and multiperiodic orbits have been observed only

for the magnetization components. We found that the increase of the Josephson frequency shrinks the magnetization trajectory in space.

The chaotic behavior driven by external periodic drive have also been investigated. In this case the system shows the increase of the Josephson to magnetic energy ratio intervals of the chaotic response and the high order modes of periodic motion near the resonance. The long-term quasiperiodic behavior is manifested in the magnetization dynamics far from the resonance. In addition to this, it was found that the variation in the amplitude of the external periodic drive leads to the chaotic behavior of the system. Therefore, by applying external periodic drive one can control the dynamical behaviour of the system.

We have emphasized that the system of NM-JJ evinced nonlinear and chaotic phenomena, where a small quantitative change in the system parameters caused a huge qualitative change in the system response. Our findings can be extended to the other system of superconducting spintronics like φ_0 -junction, which has the same current phase relation. We assume that our study will facilitate the new experimental research in this field. In particular, it might be of considerable importance for experiments on ferromagnetic resonance problems, and development of superconducting spintronics devices.

VI. ACKNOWLEDGEMENTS

The authors are grateful to I.R. Rahmonov and A.A.Mazanik for fruitful discussion of the results of this paper. The study was carried out within the framework of the Egypt-JINR research projects. Numerical simulations were funded by the project 18-71-10095 of the Russian Scientific Fund. Special thanks to Bibliotheca Alexandrina (Egypt) and JINR (Russia) HPC for the calculating servers.

-
- [1] A. Hirohata, K. Yamada, Y. Nakatani, I. L. Prejbeanu, B. Diény, P. Pirro, and B. Hillebrands, *J. Magn. Magn. Mater.* **509**, 166711 (2020).
 - [2] A. Golubov and M. Yu. Kupriyanov, *Nat. Mater.* **16**, 156 (2017).
 - [3] J. Linder and J. W. A. Robinson, *Nat. Phys.* **11**, 307 (2015).
 - [4] A. R. Rocha, V. M. García-Suárez, S. W. Bailey, C. J. Lambert, J. Ferrer AND S. Sanvito, *Nat. Mat.* **4**, 335 (2005).
 - [5] L. Bogani, and W. Wernsdorfer, *Nature Mater.* **7**, 179 (2008).
 - [6] A. Candini, S. Klyatskaya, M. Ruben, W. Wernsdorfer, and M. Affronte, *Nano Lett.*, **11** (7), 2634-2639 (2011).
 - [7] A. Ardavan, O. Rival, J. J. L. Morton, S. J. Blundell, A. M. Tyryshkin, G. A. Timco, and R. E. P. Winpenny, *Phys. Rev. Lett.* **98**, 057201 (2007).
 - [8] R. Ghosh, M. Maiti, Yu. M. Shukrinov, and K. Sengupta, *Phys. Rev. B* **96**, 174517 (2017).
 - [9] G. A. Cirillo, G. Turvani and M. Graziano, *IEEE Transactions on Nanotechnology*, vol. 18, pp. 1027-1039 (2019).
 - [10] A. Chiesa, E. Macaluso, F. Petiziol, S. Wimberger, P. Santini, and S. Carretta, *J. Phys. Chem. Lett.*, **11**, **20**, 8610-8615 (2020).
 - [11] Yu. M. Shukrinov, M. Nashaat, I. R. Rahmonov, and K. V. Kulikov, *JETP Letters*, **110**, 3, 160-165 (2019).
 - [12] Liufei Cai and E. M. Chudnovsky, *Phys. Rev. B* **82**, 104429 (2010).
 - [13] M. Lakshmanan, *Phil. Trans. R. Soc. A* **369**, 1280-1300 (2011).
 - [14] W. Buckel and R. Kleiner, *Superconductivity: Fundamentals and Applications* (Wiley-VCH, 2004).

- [15] A. Buzdin, Phys. Rev. Lett. **101**, 107005 (2008).
- [16] M. Nashaat, I. V. Bobkova, A. M. Bobkov, Yu. M. Shukrinov, I. R. Rahmonov, and K. Sengupta, Phys. Rev. B **100**, 054506 (2019).
- [17] M. Weides, M. Kemmler, H. Kohlstedt, R. Waser, D. Koelle, R. Kleiner, and E. Goldobin, Phys. Rev. Lett. **97**, 247001 (2006).
- [18] J. Pfeiffer, M. Kemmler, D. Koelle, R. Kleiner, E. Goldobin, M. Weides, A. K. Feofanov, J. Lisenfeld, and A. V. Ustinov Phys. Rev. B **77**, 214506 (2008).
- [19] A. F. Volkov and K. B. Efetov, Phys. Rev. Lett. **103**, 037003 (2009).
- [20] G. Wild, C. Probst, A. Marx, and R. Gross, Eur. Phys. J. B **78**, 509-523 (2010).
- [21] M. Kemmler, M. Weides, M. Weiler, M. Opel, S. T. B. Goennenwein, A. S. Vasenko, A. A. Golubov, H. Kohlstedt, D. Koelle, R. Kleiner, and E. Goldobin, Phys. Rev. B **81**, 054522 (2010).
- [22] S. Hikino, M. Mori, S. Takahashi and S. Maekawa, Supercond. Sci. Technol. **24**, 024008 (2011).
- [23] S. Mai, E. Kandelaki, A. F. Volkov, and K. B. Efetov, Phys. Rev. B **84**, 144519 (2011).
- [24] M. Nashaat, A. E. Botha, and Yu. M. Shukrinov, Phys. Rev. B **97**, 224514 (2018).
- [25] A. I. Buzdin, Rev. Mod. Phys. **77**, 935 (2005).
- [26] A. Moor, A. F. Volkov, and K. B. Efetov, Phys. Rev. B **92**, 214510 (2015).
- [27] S. Mironov and A. Buzdin, Phys. Rev. B **92**, 184506 (2015).
- [28] M. A. Silaev, I. V. Tokatly, and F. S. Bergeret, Phys. Rev. B **95**, 184508 (2017).
- [29] I. V. Bobkova, A. M. Bobkov, and M. A. Silaev, Phys. Rev. B **96**, 094506 (2017).
- [30] Yu. M. Shukrinov, I. R. Rahmonov, K. Sengupta, and A. Buzdin, Appl. Phys. Lett. **110**, 182407 (2017).
- [31] D. S. Rabinovich, I. V. Bobkova, A. M. Bobkov, and M. A. Silaev, Phys. Rev. B **98**, 184511 (2018).
- [32] A. A. Golubov, M. Yu. Kupriyanov, and E. Ilchev, Rev. Mod. Phys. **76**, 411 (2004).
- [33] J. Linder and K. Halterman, Phys. Rev. B **90**, 104502 (2014).
- [34] Yu. M. Shukrinov, A. Mazanik, I. R. Rahmonov, A. E. Botha and A. Buzdin, EPL, **122**, 3, 37001, (2018).
- [35] K. V. Kulikov, D. V. Anghel, A. T. Preda, M. Nashaat, M. Sameh, Yu. M. Shukrinov, arXiv:2107.01882 (2021).
- [36] L. D. Landau and E. Lifshitz, Phys. Z. Sowjetunion **8**, 153 (1935).
- [37] T. L. Gilbert, IEEE Trans. Magn. **40**, 3443 (2004).
- [38] J. A. Vélez, J. Bragard, L. M. Pérez, A. M. Cabanas, O. J. Suarez, D. Laroze, and H. L. Mancini, Chaos **30**, 093112 (2020).
- [39] A. M. Feron and R. E. Camley, Phys. Rev. B **95**, 104421 (2017).
- [40] P. Mangin, R. Kahn, *Superconductivity: an introduction*, Springer, (2016).
- [41] R. P. Cowburn, A. O. Adeyeye and M. E. Welland, New Jour. of Phys. **1**(1), 16 (1999).
- [42] L. F. Yin Phys. Rev. Lett. **97**, 067203 (2006).
- [43] K. H. J. Buschow, Concise *Encyclopedia of Magnetic and Superconducting Materials* (2005).
- [44] I. Nekrashevich, D. Litvinov, AIP Advances **8**, 085002 (2018).
- [45] J.-L. D'ejardin, A. Franco, F. Vernay, and H. Kachkachi, Phys. Rev. B **97**, 224407 (2018).
- [46] P. K. Atanasova, S. A. Panayotova, E. V. Zemlyanaya, Yu. M. Shukrinov, and I. R. Rahmonov, Lect. Notes Comput. Sci. **11189**, 301 (2019).